Analytic modelling of drying of porous materials

EINDHOVEN UNIVERSITY OF TECHNOLOGY
Department of Mathematics and Computing Science

RANA 99-29
September 1999

Analytic Modelling of Drying of Porous Materials

by

K.A. Landman, L. Pel, E.F. Kaasschieter

Reports on Applied and Numerical Analysis
Department of Mathematics and Computing Science
Eindhoven University of Technology
P.O. Box 513
5600 MB Eindhoven, The Netherlands
ISSN: 0926-4507

Analytic Modelling of Drying of Porous Materials

K.A. Landman
Department of Mathematics and Statistics
University of Melbourne
Parkville Victoria 3052, Australia
k.landman@ms.unimelb.edu.au

L. Pel
Department of Physics
Eindhoven University of Technology
P.O. Box 513, 5600 MB Eindhoven, The Netherlands
l.pel@phys.tue.nl

E.F. Kaasschieter
Department of Mathematics and Computing Science
Eindhoven University of Technology
P.O. Box 513, 5600 MB Eindhoven, The Netherlands
e.f.kaasschieter@tue.nl

Abstract

Recent experimental data by Pel has revealed the spatial and temporal structure of the moisture content during the drying process within building materials such as bricks. A simple model of the water motion is presented, guided by the observed behaviour, which allows for non-linear diffusion within the brick and a mass transfer coefficient to represent the moisture transfer between the external air current over the brick. An approximate analytic solution to the model is developed, giving the moisture profiles evolving with time. This gives insight into the different phases of the process, which consists of a rapid decrease in the moisture content in a relatively uniform manner, followed by the development of a drying front which moves with constant speed into the brick. The analytic results compare very well to the numerical solution of the equations and the experimental results.

Keywords: non-linear diffusion, drying, moisture content, analytic model, porous materials.

1 Introduction

The drying of porous media arises in various contexts in chemical engineering, civil engineering and soil science. Various models have been proposed to describe moisture transport during drying – for example, those of Philip and de Vries [20], Whitaker [27], Berger and Pei [2], Stanish [22] and Bear [1]. These models each handle the moisture flux in an individual way and a comparison between the various models can be found in Vafai and Sozen [25] and Waananen *et al* [26].

Although all these models provide further insight into moisture transport, both moisture-vapour interactions and effects of hysteresis on moisture transport are still not yet fully understood. Therefore the various input parameters must be determined experimentally, which is very time consuming work. To overcome this constraint in engineering applications, a so-called lumped model is used with the consequence that the moisture transport is described by a non-linear diffusion equation. All transport processes both in liquid and vapour phase are lumped together in one overall moisture diffusivity which is a function of the moisture content. This function must be determined experimentally.

Often drying curves which describe the total mass of water as a function of time are used to characterise the drying behaviour of materials. Such drying curves are used to determine the diffusivity function. However in analysing the drying curves, a form for the functional relationship between the moisture diffusivity coefficient and the moisture content must be assumed *a priori* (e.g. an exponential form as $D = D_0 e^{b\theta}$). Then the parameters (D_0, b) are chosen to fit the drying curve data. Therefore, this method can give an incorrect estimate of the moisture diffusivity [22].

By measuring dynamic moisture profiles during the drying process, the moisture diffusivity coefficient can be determined directly. In the past, it has been very difficult to measure these profiles non-destructively. Recently, NMR (nuclear magnetic resonance) techniques have been shown to be an excellent technique for determining these profiles during various transport processes [3, 10, 13, 14, 21, 23, 24].

Pel *et al*, [13, 14], have studied the drying of various building materials using NMR techniques. A cylindrical sample is placed in a teflon holder, with air blown over the exposed upper side. This creates a one-dimensional drying process. Figure 1 illustrates the measured moisture profiles during the drying of a fired-clay brick sample – two stages can be clearly distinguished. During the initial stage the profiles are almost uniform and the drying is externally limited by the mass transfer coefficient and air flow. In the second stage a drying front develops and moves into the brick and now the drying is internally limited. Using the profiles, the moisture diffusivity as a function of moisture content can be determined as shown in Figure 2 for this experiment. There is a clear and deep minimum in the moisture diffusivity, occurring at a moisture content denoted by θ_m. The minimum exists at the transition between liquid dominated moisture transport ($\theta > \theta_m$) and vapour

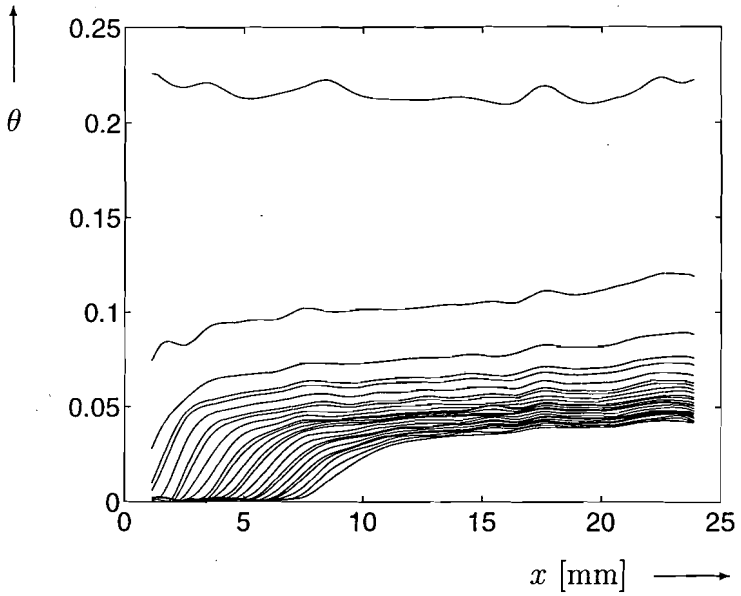

Figure 1: Typical moisture profiles with time for a fired-clay brick. The time between subsequent profiles is 2 hours.

dominated moisture transport ($\theta < \theta_m$) [13]. By examining Figure 1 in more detail, the drying front appears to move linearly with time. It is convenient to use θ_m as a marker for the position of the drying front. In Figure 3 the position of this marker is given as a function of time for drying experiments of various building materials, not just fired-clay brick. In all cases a linear relation is found. In [13, 14], Pel uses this constant speed of the drying front to more accurately approximate the moisture diffusivity at low moisture contents $\theta < \theta_m$.

Using such an experimentally determined moisture diffusivity function, the drying moisture profiles can be calculated by solving numerically the non-linear diffusion equations describing the drying proces. The resulting moisture content solutions are illustrated in Figure 4. Clearly, the calculations approximate the experimental data very well. Such simulations have been carried out for bricks of various dimensions and they all exhibit the experimentally observed drying front which moves linearly with time. This confirms that the diffusion modelling is consistent. By solving such non-linear diffusion equations with boundary conditions relevant to this drying problem, it can be verified that if the diffusivity function has a deep interior minimum, then the moisture profiles always exhibit a front which appears to move approximately linearly with time. However, if the diffusivity function is a monotonically increasing function, no such fronts exist.

Numerical simulations provide no basic understanding of the drying process, the moisture profile structure or the parameter dependence of the front velocity. Only an analytic solution can provide such an understanding, but such solutions can only be found for very

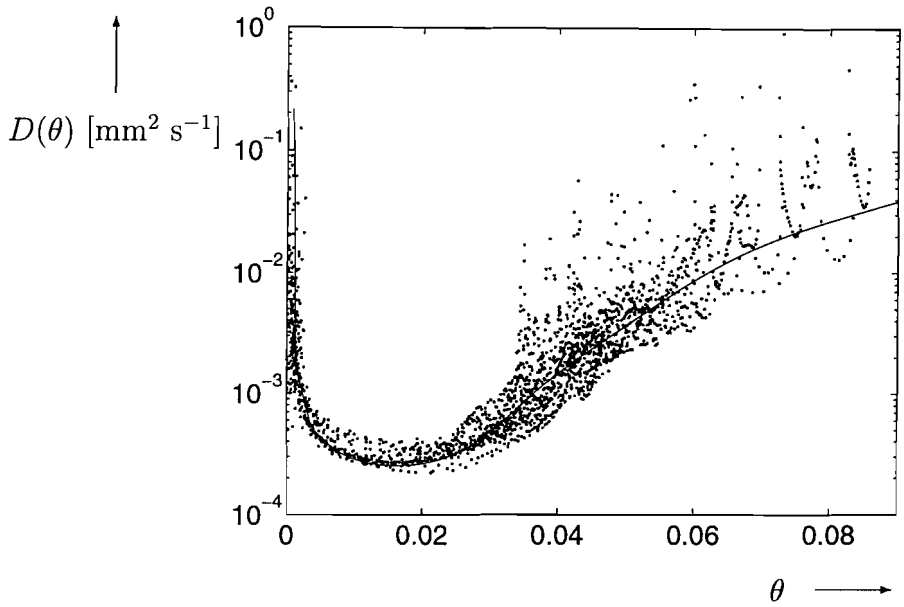

Figure 2: Typical moisture diffusivity function as a function of moisture content. Experimental estimates (dots) and fitted curve (solid line) used in Figure 4.

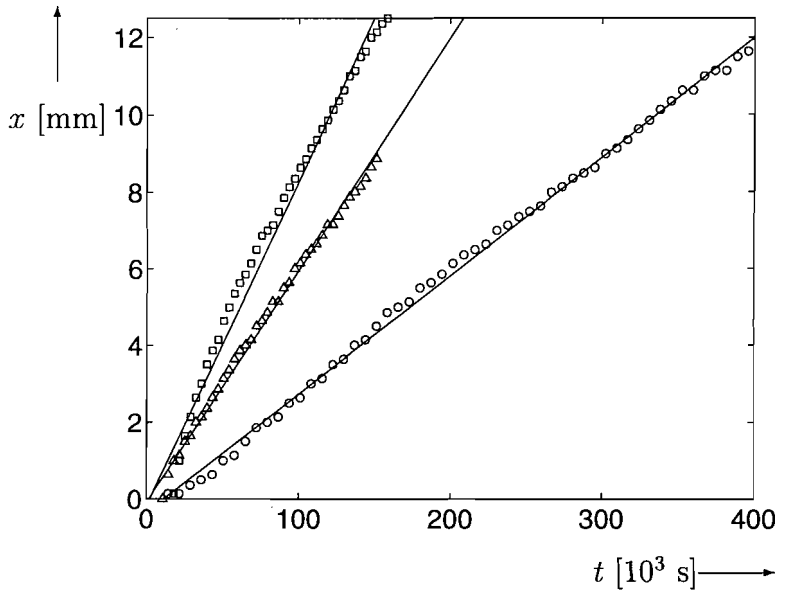

Figure 3: Position of the marker indicating the drying front with time for various building materials, i.e. gypsum (□), fired-clay brick (△) and sand-lime brick (○).

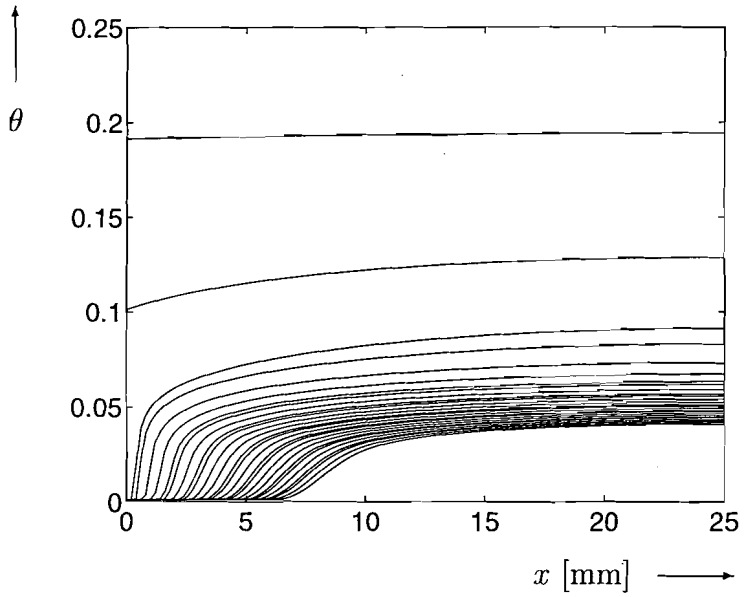

Figure 4: A numerical calculation of the moisture profiles during drying of fired-clay brick using the diffusivity fitting curve in Figure 2 and the hygroscopic curve in Figure 5. The time between subsequent profiles is 2 hours.

limited types of diffusivity functions [5, 8]. As seen for the brick experiments, the moisture diffusivity is shown experimentally to be a very strong function of moisture content, with a deep interior minimum. Therefore until now, numerical simulations have been the only means of solving the non-linear diffusion equations directly, and of reproducing the experimental profiles illustrated in Figure 1.

There are many similarities between the diffusivity function here and the ones relevant to soils. Soil diffusivity may vary by three decades and can feature a deep minimum, [18]. Much work has been done in seeking both analytic and numerical solutions of the infiltration and adsorption/desorption equations for soils. However these are most often limited to semi-infinite domains, which is not relevant here [15, 16, 17, 18, 19]. A particular finite domain problem has been considered, [4], but the functional form for $D(\theta)$ and the boundary conditions appropriate to our problem do not allow that approach to be generalised.

In this paper we will determine an approximate analytic solution to the drying problem which explains the predominant features of the experimental profiles as measured for fired-clay brick. In particular we show that the drying front movement is almost linear in time and obtain an expression for its velocity.

2 The mathematical model

Moisture transport in porous media for the one-dimensional isothermal problem that is considered here can be described by a non-linear diffusion equation on a finite domain:

$$\frac{\partial \theta}{\partial t} = \frac{\partial}{\partial x}\left(D(\theta)\frac{\partial \theta}{\partial x}\right), \; 0 < x < L \, ,$$

where θ is the volumetric moisture content, $D(\theta)$ the moisture diffusivity and L the length of the sample. In this lumped model all mechanisms for moisture transport, namely liquid flow and vapour diffusion, are combined into a single moisture diffusivity D, which is dependent on the actual moisture content. Here the influence of gravity has been neglected. As can be seen from experimental data in Figure 2, the moisture diffusivity for fired-clay brick needs to be approximated by a function with a deep interior minimum at a moisture content denoted θ_m. We will now rely on some general properties of the diffusivity function. Later we will choose a suitable function which mimics the major features of the data, but it is unnecessary to specify this now.

Initially the brick is assumed to have a constant moisture content θ_0, so that

$$\theta(x, 0) = \theta_0 \, .$$

We assume that $\theta_m \ll \theta_0$.

At the drying surface $x = 0$, air with a fixed relative humidity is blown over the brick sample. Under isothermal conditions the flux across the boundary is then given by

$$D(\theta)\frac{\partial \theta}{\partial x} = \beta(h_m(\theta) - h_a) \, , \tag{1}$$

where β is the mass transfer coefficient, h_a is the relative humidity of the blown air and $h_m(\theta)$ is the relative humidity of the material at the surface which is determined by the desorption isotherm (also called hygroscopic curve). For the fired-clay brick discussed in this paper, the desorption curve is a monotonically increasing function with $h_m(\theta_0) = 1$ as given in Figure 5. We further define θ_∞ to be the moisture content which matches the external surface air-humidity, namely

$$h_m(\theta_\infty) = h_a \, . \tag{2}$$

Clearly for drying we require $\theta_\infty < \theta_0$.

The minimum value of the diffusivity occurs at θ_m and equals

$$D(\theta_m) = \min_{\theta_\infty \le \theta \le \theta_0} D(\theta) \, . \tag{3}$$

Hence if $\theta_\infty < \theta_m$, the diffusivity function $D(\theta)$ will exhibit an interior minimum over the range of values of θ that are of interest. For comparison later, we will consider the limiting

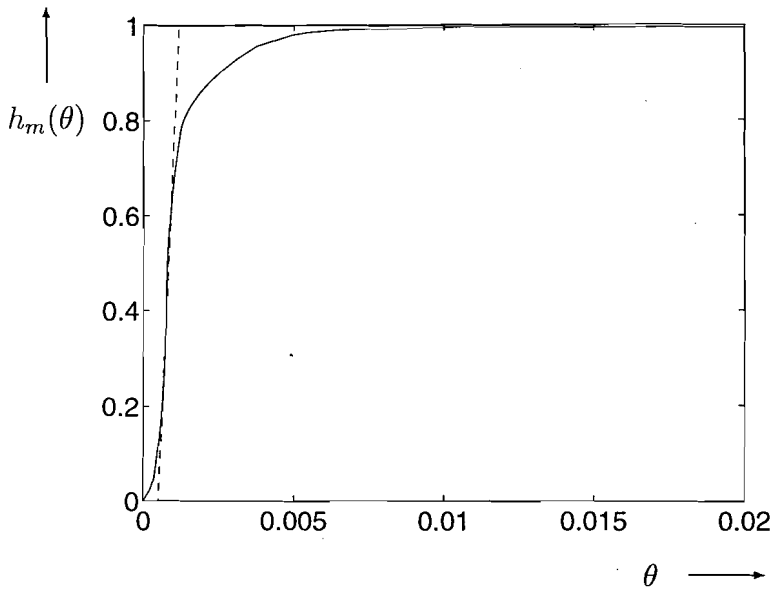

Figure 5: Typical hygroscopic curve (solid line) for fired clay brick, showing the linear approximation at θ_∞ (dashed line).

case $\theta_\infty = \theta_m$ where the diffusivity has no interior minimum. Hence, here we assume that $\theta_\infty \leq \theta_m \ll \theta_0$.

At the boundary $x = L$ there is no moisture flux, so that

$$\frac{\partial \theta}{\partial x}(L,t) = 0 \, .$$

It should be noted in particular that the moisture content is not fixed at either of the two boundaries.

The problem formulated here differs from many wetting or drying (adsorption or desorption) problems often considered. The most common scenario involves the non-linear moisture-dependent diffusion equation over a semi-infinite domain with a uniform initial moisture content and a fixed moisture content boundary condition at the exposed end $x = 0$. For these problems, the Boltzmann transformation $\phi = x/\sqrt{t}$ reduces the equations to an ordinary differential equation such that $\theta = \theta(\phi)$, or alternatively this can be written as $\phi = \phi(\theta)$. This is true for any $D(\theta)$ form, although solutions will have to be attained numerically, except for special class of $D(\theta)$ forms [17, 18]. An important consequence of the solution form is that the position where the moisture content equals a specified value $\theta = \theta^*$ say, must move like $\sqrt{t}$.

Now let us turn to finite domain problems. During the early stages in adsorption or wetting problems, the moisture moves in at $x = 0$ and the moisture is not aware that

the region is of finite extent, and the problem behaves as if semi-infinite in extent. Hence during the early stages, the Boltzmann transformation is appropriate and $\sqrt{t}$ behaviour is expected and observed [13]. Even though the Boltzmann transformation works initially, eventually the moisture reaches towards the far boundary $x = L$, and the applied boundary condition is noticed and affects the profile shape. The behaviour will no longer be described by $\sqrt{t}$. Recent examples studying wetting of cereal grains show that after this early stage the behaviour is linear in time [11, 12].

The wetting problem with the so-called porous media equations, with $D(\theta) = \theta^n$ and $\theta = 0$ initially, has been much studied. For infinite-domain problems, some solutions with a front defining wet ($\theta > 0$) and dry ($\theta = 0$) regions moves like $t^{1/(2+n)}$. As n becomes large, the moisture profile looks more like a flat plateau with very sharp fronts, called a mesa [9]. The finite domain version of this problem gives $\sqrt{t}$ behaviour for the initial stages until the front hits the far boundary, and then the time behaviour switches to a linear behaviour in t [28, 29].

Desorption or drying problems are inherently different from adsorption or wetting problems, even in the early time stages. In the semi-infinite problem, if moisture is removed from $x = 0$, we must always assume that there is a source of moisture at infinity, since the moisture content far upstream always equals the initial value. (Note the important fact that such a region can never dry.) Hence, a drying problem on a finite domain *cannot* be approximated by a semi-infinite domain, even in the early stages. Therefore the Boltzmann transformation and $\sqrt{t}$ implications to the solutions cannot be anticipated for the problem we are considering in this paper.

Here we develop an approximate analytic solution for the moisture profiles evolving with time. We first discuss the effect of the boundary conditions and show that this gives two predominant time regimes in this problem, leading to the two drying stages outlined previously. The real interest lies in the second stage when the drying front develops. We will find that the drying front does not move with $\sqrt{t}$ behaviour.

3 Early time behaviour

The early time solution is governed by the mass transfer boundary condition at the drying surface, namely equation (1).

For early times, when θ starts at θ_0 and remains such that $\theta \gg \theta_m$, $h_m(\theta)$ can be readily approximated by a straight line as

$$h_m(\theta) = h_m(\theta_0) + h'_m(\theta_0)(\theta - \theta_0) \,, \tag{4}$$

where $h'_m(\theta_0) > 0$. Then the surface resistance boundary condition (1) becomes

$$D(\theta)\frac{\partial \theta}{\partial x} = \beta h'_m(\theta_0)(\theta - \theta_1) \,,$$

where here

$$\theta_1 = \theta_0 - \frac{h_m(\theta_0) - h_a}{h'_m(\theta_0)} .$$

The reduction of the total moisture content in the material must balance the outward flux through the surface $x = 0$, namely

$$\frac{d}{dt}\int_0^L \theta(x)\, dx = -\beta h'_m(\theta_0)(\theta(0) - \theta_1) .$$

Hence for this early time stage, we can associate a time scale with the surface resistance as $L/\left(\beta h'_m(\theta_0)\right)$.

At the same time, diffusion processes are taking place within the brick. The corresponding time scale, when θ is close to θ_0 is $L^2/D(\theta_0)$. To compare the diffusion time scale to the surface resistance time scale, we form their ratio, which introduces a dimensionless parameter λ defined as

$$\lambda = \frac{\beta L h'_m(\theta_0)}{D(\theta_0)} .$$

Using the values in Table 1 for fired-clay brick, the initial diffusion time scale is very small, while the surface resistance time scale is approximately 18 hours. Hence their ratio $\lambda \approx 2{\cdot}10^{-3}$, so that λ is much smaller than unity. In this initial time regime, θ may decrease from θ_0 to say 0.1, so that at this θ value, the diffusion time scale is then approximately 1.7 hours, still giving a very small value for λ. Hence it is appropriate to consider these equations for the small λ limit, which says that the diffusion time scale is much shorter than the surface resistance time scale. We can then expect that over the surface resistance time scale the moisture content is in diffusive equilibrium. This is called the *pseudo-steady state solution.* Hence for the early stages of the drying process, the appropriate time scale is *not* the diffusion time scale but the surface resistance time scale. This means that the early stages are externally driven by the surface boundary condition, and not internally limited by the diffusion process. This is now explored further.

These arguments require us to scale the equations with the surface resistance time scale, relevant to θ near θ_0 and to this end we introduce dimensionless parameters

$$\xi = \frac{x}{L} \quad , \quad \sigma = \frac{\beta h'_m(\theta_0) t}{L} \quad , \quad \Gamma(\theta) = \frac{D(\theta)}{D(\theta_0)} ,$$

giving the drying problem equations as

$$\lambda \frac{\partial \theta}{\partial \sigma} = \frac{\partial}{\partial \xi}\left(\Gamma(\theta)\frac{\partial \theta}{\partial \xi}\right) \quad , \quad 0 < \xi < 1 , \tag{5}$$

$$\Gamma(\theta)\frac{\partial \theta}{\partial \xi} = \lambda(\theta - \theta_1) \text{ at } \xi = 0 \quad , \quad \frac{\partial \theta}{\partial \xi}(1, \sigma) = 0 , \tag{6}$$

$$\theta(\xi, 0) = \theta_0 . \tag{7}$$

The solution to these equations can be found using a perturbation expansion in the small parameter λ as

$$\theta = \psi_0 + \lambda\psi_1 + \lambda^2\psi_2 + \dots \ .$$

Collecting together terms of like powers of λ, yields at the lowest order (namely $\mathcal{O}(1)$) the following system:

$$\frac{\partial}{\partial\xi}\left(\Gamma(\psi_0)\frac{\partial\psi_0}{\partial\xi}\right) = 0 \quad , \quad 0 < \xi < 1 \ , \tag{8}$$

$$\Gamma(\psi_0)\frac{\partial\psi_0}{\partial\xi}(0,\sigma) = 0 \quad , \quad \frac{\partial\psi_0}{\partial\xi}(1,\sigma) = 0 \ , \tag{9}$$

$$\psi_0(\xi,0) = \theta_0 \ .$$

The solution to the partial differential equation (8) is easily found to be

$$\Gamma(\psi_0)\frac{\partial\psi_0}{\partial\xi} = F(\sigma) \ ,$$

where $F(\sigma)$ is an arbitrary function of dimensionless time σ. However from (9), the flux must equal zero at both endpoints, hence $F(\sigma) = 0$. This implies that ψ_0 must be a function of σ only and independent of ξ, namely

$$\psi_0 = \psi_0(\sigma) \ .$$

In order to determine this function of σ, we need to collect together terms of $\mathcal{O}(\lambda)$ from equations (5)–(7). Using the fact that ψ_0 is independent of ξ, we obtain

$$\frac{d\psi_0}{d\sigma} = \frac{\partial}{\partial\xi}\left(\Gamma(\psi_0)\frac{\partial\psi_1}{\partial\xi}\right), \ 0 < \xi < 1 \ , \quad . \tag{10}$$

$$\Gamma(\psi_0)\frac{\partial\psi_1}{\partial\xi} = \psi_0 - \theta_1 \text{ at } \xi = 0 \quad , \quad \frac{\partial\psi_1}{\partial\xi}(1,\sigma) = 0 \ , \tag{11}$$

$$\psi_1(\xi,0) = 0 \ . \tag{12}$$

We first integrate the differential equation to give

$$\int_0^1 \frac{d\psi_0}{d\sigma}d\xi = \frac{d\psi_0}{d\sigma} = \int_0^1 \frac{\partial}{\partial\xi}\left(\Gamma(\psi_0)\frac{\partial\psi_1}{\partial\xi}\right)d\xi \ .$$

Evaluation of the right-hand side gives the difference in the known fluxes at the two endpoints, namely

$$\frac{d\psi_0}{d\sigma} = \theta_1 - \psi_0 \ .$$

Integrating this and using the initial condition (12) gives

$$\psi_0(\sigma) = \theta_1 + (\theta_0 - \theta_1)e^{-\sigma} \ .$$

The ξ dependence in θ only appears at $\mathcal{O}(\lambda)$ in the $\psi_1(\xi,\sigma)$ term. From (10) it can be seen that $\partial^2\psi_1/\partial\xi^2$ is a known (negative) function of σ and is independent of ξ. Hence integration twice with respect to ξ will yield that ψ_1 is a quadratic in ξ. From (10)–(11) it follows that

$$\psi_1(\xi,\sigma) = \frac{\theta_0-\theta_1}{\Gamma(\psi_0)} e^{-\sigma}\left(\xi - \frac{1}{2}\xi^2 + K(\sigma)\right) ,$$

where $K(\sigma)$ can be determined from the terms of $\mathcal{O}(\lambda^2)$ from equations (5)–(7).

Therefore for this initial drying stage, at the lowest order in λ the moisture profiles are uniform in space and decrease exponentially with time. The $\mathcal{O}(\lambda)$ perturbation to the spatially uniform profiles is quadratic in ξ. This model explains the externally limited early time behaviour of the profiles.

It is worth noting that the exact form of $D(\theta)$ is irrelevant here – only the relative size of $D(\theta_0)$ is important, as indicated in the parameter λ. Hence this type of early time behaviour occurs as long as $\lambda \ll 1$ and is independent of whether $D(\theta)$ has an internal minimum or not, given our assumption that $\theta_m \ll \theta_0$.

However, even with $\lambda \ll 1$, the approximations we have made are only valid when the linear approximation (4) for h_m around θ_0 is valid and $\theta_0 > \theta_1$. When these approximations are no longer valid, the moisture content at the drying surface starts to decrease rapidly in time, which gives rise to a large moisture content gradient at the surface. When this occurs, the surface boundary condition no longer behaves like a surface resistance condition. This is considered next.

4 Later time behaviour

For surface values of θ close to the moisture content which matches the external air-humidity, a linear approximation to $h_m(\theta)$ around θ_∞ is now appropriate, as seen in Figure 5. Using (2) this can be written as

$$h_m(\theta) = h_a + h'_m(\theta_\infty)(\theta - \theta_\infty) .$$

It is expected that the minimum diffusivity $D(\theta_m)$, as defined in (3), is the diffusivity value controlling the time scale of the drying process, so that the representative time scale for this stage of the drying process will be $L^2/D(\theta_m)$. We introduce the following dimensionless parameters

$$\xi = \frac{x}{L} \quad , \quad \tau = \frac{D(\theta_m)}{L^2}t \quad , \quad \Delta(\theta) = \frac{D(\theta)}{D(\theta_m)} ,$$

giving the drying equations at this stage as

$$\begin{aligned}
&\frac{\partial\theta}{\partial\tau} = \frac{\partial}{\partial\xi}\left(\Delta(\theta)\frac{\partial\theta}{\partial\xi}\right), \ 0<\xi<1\,, \\
&\gamma\Delta(\theta)\frac{\partial\theta}{\partial\xi} = \theta-\theta_\infty \text{ at } \xi=0 \quad , \quad \frac{\partial\theta}{\partial\xi}(1,\tau)=0\,, \\
&\theta(\xi,0)=\theta_0, \ 0<\xi<1\,.
\end{aligned} \tag{13}$$

Here we have introduced the dimensionless parameter γ defined as

$$\gamma = \frac{D(\theta_m)}{\beta L h'_m(\theta_\infty)}\,,$$

which equals the ratio of the surface resistance time scale to the diffusion time scale. From the parameter values in Table 2, $\gamma \approx 1\cdot 10^{-5}$, so we are now working in a regime where the surface resistance time scale is very small compared to the diffusion time scale, namely $\gamma \ll 1$. Hence in this stage of the problem the surface boundary condition acts like a fixed moisture content condition. To show this formally, we write the solution as a perturbation expansion in the small parameter γ as

$$\theta = \bar{\theta} + \gamma\psi_1 + \gamma^2\psi_2 + \ldots\,. \tag{14}$$

Collecting together terms of like powers of γ, yields at the lowest order in γ (namely $\mathcal{O}(1)$) the following system:

$$\frac{\partial\bar{\theta}}{\partial\tau} = \frac{\partial}{\partial\xi}\left(\Delta(\bar{\theta})\frac{\partial\bar{\theta}}{\partial\xi}\right), \ 0<\xi<1\,, \tag{15}$$

$$\bar{\theta}(0,\tau)=\theta_\infty \quad , \quad \frac{\partial\bar{\theta}}{\partial\xi}(1,\tau)=0\,, \tag{16}$$

$$\bar{\theta}(\xi,0)=\theta_0\,.$$

It should be noted that in going from (13) to (16), we must ensure that the value of $\gamma\Delta(\theta_\infty) = \gamma D(\theta_\infty)/D(\theta_m) \ll 1$. This is indeed the case here.

Since $\gamma \ll 1$, the lowest order term in the expansion (14), namely $\bar{\theta}$, provides an excellent approximation to θ. We are now required to find solutions to this new problem, one with a fixed moisture content condition at one end, and a no-flux condition at the other end. Clearly the moisture content $\bar{\theta}(1,\tau)$ decreases with time, and the equilibrium solution is $\bar{\theta}\to\theta_\infty$ over all ξ values.

5 Asymptotic analysis

As discussed above, the later time behaviour for the drying problem reduces to the system (15)–(16). In this section, we will show how a steady state approximation is the key to

obtaining an understanding of the moisture profiles.

Experimental evidence for the drying process has established that the moisture diffusivity is a highly non-linear function as illustrated in Figure 2. This means that the scaled diffusivity $\Delta(\bar{\theta})$ will change by two orders of magnitude over the moisture content range. Hence, certainly for any $\bar{\theta}$ value not close to θ_m, $\Delta(\bar{\theta}) \gg 1$. Over the time scale we are studying, the left-hand side of (15) is $\mathcal{O}(1)$ while the size of $\Delta(\bar{\theta})$ implies that the right-hand side of (15) is much larger. Hence, relative to the right-hand side, the left-hand side can be approximated to zero. (We can make this formal by using a regular perturbation expansion.) This implies that the system is effectively in diffusive equilibrium at every value of time τ. This behaviour is known as the pseudo-steady state, because the solution is still a function of time but satisfies the diffusive equilibrium equations. Similar considerations have been used in a wetting problem on a finite domain [11, 12] . These arguments will help motivate the analysis below.

Notice that if we neglect the time dependent derivative in (15) *and* satisfy (16), then the pseudo-steady state solution is in fact the final equilibrium solution $\bar{\theta} = \theta_\infty$. Therefore in order to consider the pseudo-steady state conditions for any particular time, we need to recall that the moisture can only leave the brick at the drying boundary $\xi = 0$. We denote this, as yet, undetermined flux by

$$G(\tau) = \Delta(\theta_\infty)\frac{\partial \bar{\theta}}{\partial \xi}(0,\tau) \; . \tag{17}$$

To determine the outward flux $G(\tau)$ we consider the reduction to the total moisture content. Using (15) and the flux values at the endpoints (16) and (17) gives

$$\frac{d}{d\tau}\int_0^1 \bar{\theta}\, d\xi = \int_0^1 \frac{\partial \bar{\theta}}{\partial \tau}\, d\xi = \int_0^1 \frac{\partial}{\partial \xi}\left(\Delta(\bar{\theta})\frac{\partial \bar{\theta}}{\partial \xi}\right) d\xi = -G(\tau) \; . \tag{18}$$

Motivated by our previous arguments, we now formulate the appropriate pseudo-steady state problem and let ψ be its solution, namely

$$\begin{aligned} &\frac{\partial}{\partial \xi}\left(\Delta(\psi)\frac{\partial \psi}{\partial \xi}\right) = 0 \quad , \quad 0 < \xi < 1, \\ &\psi(0,\tau) = \theta_\infty \quad , \quad \Delta(\psi)\frac{\partial \psi}{\partial \xi} = G(\tau) \quad \text{at } \xi = 0 \; . \end{aligned} \tag{19}$$

If we introduce the Kirchoff transformation, [6], and define a function $V(\psi)$ as

$$V(\psi) = \int_{\theta_m}^{\psi} \Delta(\phi)\, d\phi \; , \tag{20}$$

then the differential equation (19) reduces to the Laplace equation

$$\frac{\partial}{\partial \xi}\left(\Delta(\psi)\frac{\partial \psi}{\partial \xi}\right) = \frac{\partial^2 V(\psi)}{\partial \xi^2} = 0 \; .$$

Using the boundary conditions at $\xi = 0$, this equation simply integrates to

$$V(\psi) = G(\tau)\xi - U \,, \tag{21}$$

where

$$U = -V(\theta_\infty) = \int_{\theta_\infty}^{\theta_m} \Delta(\theta)\, d\theta \geq 0 \,,$$

since $\theta_\infty \leq \theta_m$. In general to obtain the solution ψ, we must invert the function V to give

$$\psi = V^{-1}(G(\tau)\xi - U) \,. \tag{22}$$

We wish to rewrite the equation determining the surface flux in terms of the pseudo-steady state solution ψ. Equation (18) can be written as

$$\int_0^1 \frac{\partial \psi}{\partial \tau}\, d\xi = -G(\tau) + \int_0^1 \frac{\partial(\psi - \bar{\theta})}{\partial \tau}\, d\xi \,. \tag{23}$$

We assume here that

$$\left| \int_0^1 \frac{\partial(\psi - \bar{\theta})}{\partial \tau}\, d\xi \right| = \left| \frac{d}{d\tau} \int_0^1 (\psi - \bar{\theta})\, d\xi \right| \ll G(\tau) \,. \tag{24}$$

This integral term can be interpreted as the time rate of change of the difference in the total moisture content of the pseudo-steady state solution ψ and the full drying solution $\bar{\theta}$.

Assuming we can neglect the integral term on the right-hand side of (23) compared to $G(\tau)$, we obtain the approximation

$$\int_0^1 \frac{\partial \psi}{\partial \tau}\, d\xi = -G(\tau) \,. \tag{25}$$

Given the solution ψ given in (22), we will establish that $G(\tau)$ can be determined sufficiently accurately from (25). Consequently, a good approximation for the defining features of the drying problem can be deduced.

We will show that the approximation is good even though the diffusive flux for ψ is $G(\tau)$ across the whole ξ range, while the flux of $\bar{\theta}$ is not spatially uniform – it is $G(\tau)$ at the drying end and equal to zero at $\xi = 1$.

The integral term in (25) is equivalent to $\frac{d}{d\tau} \int_0^1 \psi\, d\xi$, which is the rate of change of the total moisture content in the pseudo-steady state brick. Later when we actually evaluate this equation, it turns out to be more convenient to have the form of the integral as expressed in (25).

Next we will choose particular forms for the diffusivity $D(\theta)$. This will allow the determination of $G(\tau)$, from the equation (22) for ψ as a function of $G(\tau)$. We will

apply the pseudo-steady state approximations to two typical diffusivity functions used for drying problems. We will consider two forms of the diffusion coefficient, both exponentially growing for larger values of moisture content but one will have an interior minimum and the other will not have an interior minimum. We will see that the presence of an interior minimum ensures the existence a drying front and the deeper the interior minimum the sharper the front.

6 Application to a diffusivity function with an interior minimum

As previously discussed, NMR experimental data strongly defines a diffusivity function with an internal minimum, which we denote as θ_m. Given data as in Figure 2, we could fit a functional form as

$$D(\theta) = A_1 e^{b_1\theta} + A_2 e^{-b_2\theta} ,$$

where A_1, A_2, b_1 and b_2 are positive constants. However with this functional form, the function V is not invertible. Therefore an explicit expression for ψ is not possible, making integration of (25) not possible. In order to proceed analytically and obtain explicit expressions for ψ, we use the simpler functional form which has similar features

$$D(\theta) = \begin{cases} A_1 e^{b_1\theta} , & \theta \geq \theta_m , \\ A_2 e^{-b_2\theta} , & \theta \leq \theta_m , \end{cases} \tag{26}$$

where the constants are chosen such that D is continuous at θ_m. With the values given in Table 2, the approximation is shown in Figure 6. Although the fit for $\theta < \theta_m$ is not good, the essential feature of the diffusivity function, namely the deep internal minimum, is captured in our simple function (26).

In terms of the fitting constants introduced above, θ_m is defined as

$$\theta_m = \frac{1}{b_1 + b_2} \ln\left(\frac{A_2}{A_1}\right) .$$

Typically the diffusivity changes by orders of magnitude, so b_1 and b_2 are assumed to be large. The formulation (26) can be rewritten more conveniently as

$$\Delta(\theta) = \frac{D(\theta)}{D(\theta_m)} = \begin{cases} e^{b_1(\theta-\theta_m)} , & \theta \geq \theta_m , \\ e^{-b_2(\theta-\theta_m)} , & \theta \leq \theta_m . \end{cases} \tag{27}$$

For this case, the function $V(\psi)$ as defined in (20) is

$$V(\psi) = \begin{cases} \dfrac{1}{b_1}\left(e^{b_1(\psi-\theta_m)} - 1\right) , & \psi \geq \theta_m , \\ \dfrac{1}{b_2}\left(1 - e^{-b_2(\psi-\theta_m)}\right) , & \psi \leq \theta_m . \end{cases}$$

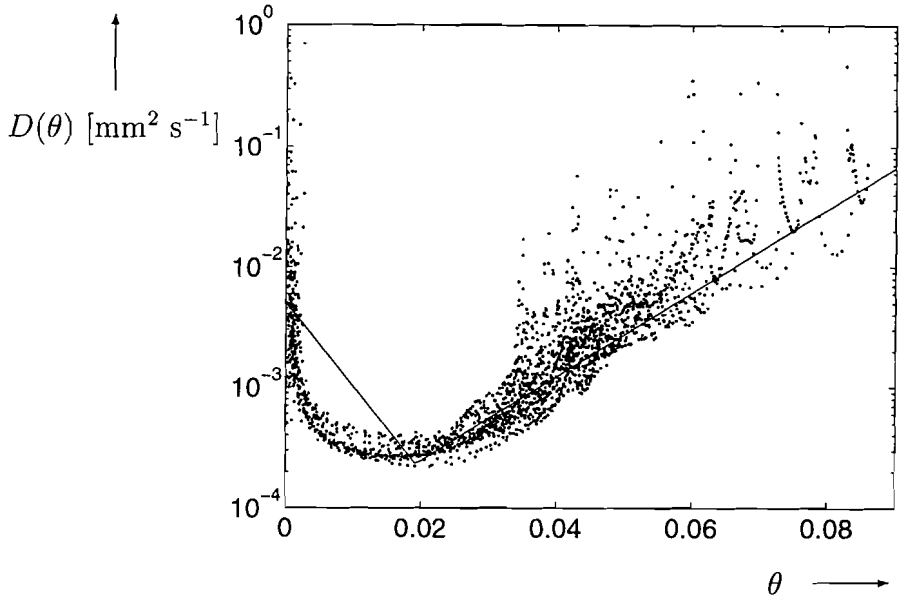

Figure 6: Simple exponential diffusivity given by (26) with Table 2 parameter values (solid line) and the experimental estimates (dots).

Hence explicit expression for ψ can be determined from (22) as

$$\psi(\xi,\tau) = \begin{cases} \theta_m + \dfrac{1}{b_1}\ln\left(1 - b_1 U + b_1 G(\tau)\xi\right) & , \quad \psi \geq \theta_m \,, \\ \theta_m - \dfrac{1}{b_2}\ln\left(1 + b_2 U - b_2 G(\tau)\xi\right) & , \quad \psi \leq \theta_m \,. \end{cases} \tag{28}$$

In Figure 7 typical pseudo-steady state moisture profiles for decreasing values of $G(\tau)$ are illustrated. Notice that the slope of the moisture profiles at first increases, reaches a maximum at $\psi = \theta_m$, where there is an inflection point, and then decreases for $\psi > \theta_m$. The slope is given by

$$\frac{\partial \psi}{\partial \xi} = \frac{G(\tau)}{\Delta(\psi)} \,, \tag{29}$$

where $\Delta(\psi)$, being the scaled diffusivity function (27), is initially a decreasing and then an increasing function. This shape for $\psi(\xi,\tau)$ as a function of ξ produces a so-called *drying front*, and we see that it moves into the material. We point out that at this stage the evolution of G with τ has not been determined. On physical grounds we expect it to be a positive decreasing function.

We can determine the position of this drying front as it moves into the brick. As noted, the slope of ψ is a maximum when $\psi = \theta_m$, and we choose this as a marker for the front position. If we denote this moving position as $\delta(\tau)$, it is then defined by

$$\psi(\delta(\tau),\tau) = \theta_m \,. \tag{30}$$

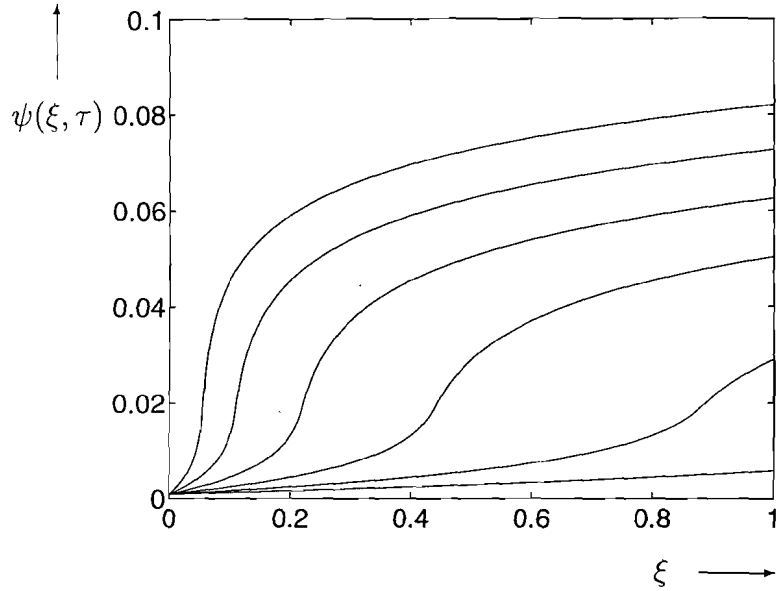

Figure 7: The moisture profile $\psi(\xi,\tau)$ for $D(\theta)$ given by (26) with Table 2 parameter values. Here $G(\tau) = 1/(b_1 g(\tau))$ has values 2, 1, 0.5, 0.25, 0.125 and 0.0625.

This definition together with (28) implies that

$$1 - b_1 U + b_1 G(\tau)\delta(\tau) = 1 \quad , \quad 1 + b_2 U - b_2 G(\tau)\delta(\tau) = 1 \, . \tag{31}$$

6.1 Determination of an equation for $G(\tau)$ and $\delta(\tau)$

We now need to determine the flux $G(\tau)$ so that the time evolution of the moisture profiles and drying front can be uniquely calculated. To do this, the time derivative of $\psi(\xi,\tau)$ given by (28) is required for the integral expression (25). To evaluate the integral, we subdivide it in the following way:

$$\int_0^1 \frac{\partial \psi}{\partial \tau}\, d\xi = \int_0^{\delta(\tau)} \frac{\partial \psi}{\partial \tau}\, d\xi + \int_{\delta(\tau)}^1 \frac{\partial \psi}{\partial \tau}\, d\xi = -G(\tau) \, . \tag{32}$$

We note from (30) that when $\theta_\infty \le \psi < \theta_m$, $0 \le \xi < \delta$, and when $\psi > \theta_m$ then $\delta < \xi < 1$. Therefore, using (28) and (31), evaluation of each of these integrals yields

$$\begin{aligned} &\int_{\delta(\tau)}^1 \frac{\partial \psi}{\partial \tau}\, d\xi = \int_{\delta(\tau)}^1 \frac{G'(\tau)\xi}{1 - b_1 U + b_1 G(\tau)\xi}\, d\xi \\ &= \frac{G'(\tau)}{b_1 G(\tau)} \left[1 - \delta(\tau) - \frac{1 - b_1 U}{b_1 G(\tau)} \ln\left(1 - b_1 U + b_1 G(\tau)\right) \right] , \end{aligned} \tag{33}$$

$$\begin{aligned} &\int_0^{\delta(\tau)} \frac{\partial \psi}{\partial \tau}\, d\xi = \int_0^{\delta(\tau)} \frac{G'(\tau)\xi}{1 + b_2 U - b_2 G(\tau)\xi}\, d\xi \\ &= \frac{G'(\tau)}{b_2 G(\tau)} \left[\frac{1 + b_2 U}{b_2 G(\tau)} \ln(1 + b_2 U) - \delta(\tau) \right] . \end{aligned} \tag{34}$$

It will be convenient to introduce the function

$$g(\tau) = \frac{1}{b_1 G(\tau)} \,. \tag{35}$$

and to write the position of the front in terms of $g(\tau)$ from (31) as

$$\delta(\tau) = \frac{U}{G(\tau)} = b_1 U g(\tau). \tag{36}$$

By introducing the constants

$$d = \frac{b_1}{b_2} \quad , \quad K_1 \equiv K_1(b_1 U) = 1 - b_1 U \quad ,$$

$$K_2 \equiv K_2(b_1 U, d) = d^2 \left(1 + \frac{b_1 U}{d}\right) \ln\left(1 + \frac{b_1 U}{d}\right) - b_1 U (1 + d) \,,$$

the equations (32)–(34) combine to give the differential equation

$$M(g)\frac{dg}{d\tau} = 1 \,, \tag{37}$$

where we have introduced the function $M(g)$ defined as

$$M(g) = 1 - K_1 g \ln\left(K_1 + \frac{1}{g}\right) + K_2 g \,.$$

Thus M is also a function of the two constants $b_1 U$ and d, through the constants K_1 and K_2.

There are restrictions to the values of g. After the early time period discussed in Section 3, at the initial time for this current stage, assigned with no loss of generality as $\tau = 0$, the out-flux $G(\tau)$ will be finite, but may be relatively large. Consequently, $g(0) > 0$ and $\delta(0) > 0$. We denote $g(0) = g_0$. Note that if the drying process was governed by the surface boundary condition $\theta(0, \tau) = \theta_\infty$ from the start when $\theta(\xi, 0) = \theta_0$, the flux $G(0)$ would be infinite, and hence $g_0 = \delta(0) = 0$. There is an upper bound on the value of g because the scaled distance must satisfy $0 < \delta < 1$. Hence combining these two bounds implies that g must fulfil $0 \leq g_0 < g < \frac{1}{b_1 U}$.

We now briefly discuss the properties of $M(g)$. With some algebra, it can be shown that

$$M(0) = 1 \quad ,$$

$$M(\frac{1}{b_1 U}) = 1 + \frac{K_2}{b_1 U} = \frac{d^2}{b_1 U}\left[\left(1 + \frac{b_1 U}{d}\right)\left(\ln(1 + \frac{b_1 U}{d}) - 1\right) + 1\right] > 0 \quad ,$$

$$M'(g) \to K_1 (1 + \ln g) + K_2 \quad \text{as} \quad g \to 0 \quad ,$$

$$M'(\frac{1}{b_1 U}) = K_1(1-K_1) + K_2 < 0 \quad ,$$

$$M''(g) = \frac{K_1}{(K_1 g + 1)^2 g} > 0 \, .$$

Hence, we can deduce the following. If $b_1 U > 1$, then $K_1 < 0$ and $M(g)$ increases, reaches a maximum, and then decreases. Its value at the end of its range satisfies $M(\frac{1}{b_1 U}) > 1$ if $K_2 > 0$; otherwise if $K_2 < 0$, then $0 < M(\frac{1}{b_1 U}) < 1$. Alternatively, if $b_1 U \leq 1$, then $K_1 \geq 0$ and $K_2 < 0$ and consequently $M(g)$ monotonically decreases to a nonnegative value. Hence for all choices of $b_1 U$ and d, the function $M(g) > 0$ for $0 < g < \frac{1}{b_1 U}$. For the parameter values appropriate to our study, we have found that $b_1 U > 1$ and $d < 1$. The positivity of M is expected, since then $\frac{dg}{d\tau} > 0$, and hence the surface flux $G(\tau)$ will be a decreasing function of time.

The equation (37) can be integrated to give

$$N(g(\tau)) = \tau + N(g_0) \, , \tag{38}$$

where

$$N(g) = \int_0^g M(f) \, df = \frac{1}{2}\left[g - K_1 g^2 \ln(K_1 + \frac{1}{g}) + \frac{1}{K_1} \ln(1 + K_1 g) + K_2 g^2 \right] \, . \tag{39}$$

Here an integration constant $N(g_0)$ has been introduced. Again we note that N is a function of the two constants $b_1 U$ and d, through the constants K_1 and K_2. Since the function $M(g) > 0$, its integral function $N(g)$ must also be a positive function.

6.2 Estimates of behaviour of $g(\tau)$ and $\delta(\tau)$

Determining g as a function of τ from (38) must be done numerically. By plotting function N for various parameter values, it appears linear over much of the domain of interest, as shown in Figure 8. From (38) we expect $g(\tau)$ to also appear linear over much of its range, as illustrated in Figure 9. Only during the initial stages does the slope appear to change.

Clearly, since the front position is determined by $\delta(\tau)$, this will also appear to move at a constant rate in time. This is exactly the type of behaviour extracted from the experimental results, and confirmed by numerical simulations.

It would be convenient to have an accurate estimate of the front position, without having to solve the non-linear equation (38) each time. Three approaches to estimating $dg/d\tau$ and hence $g(\tau)$ and $\delta(\tau)$ are given here – each has certain advantages and disadvantages.

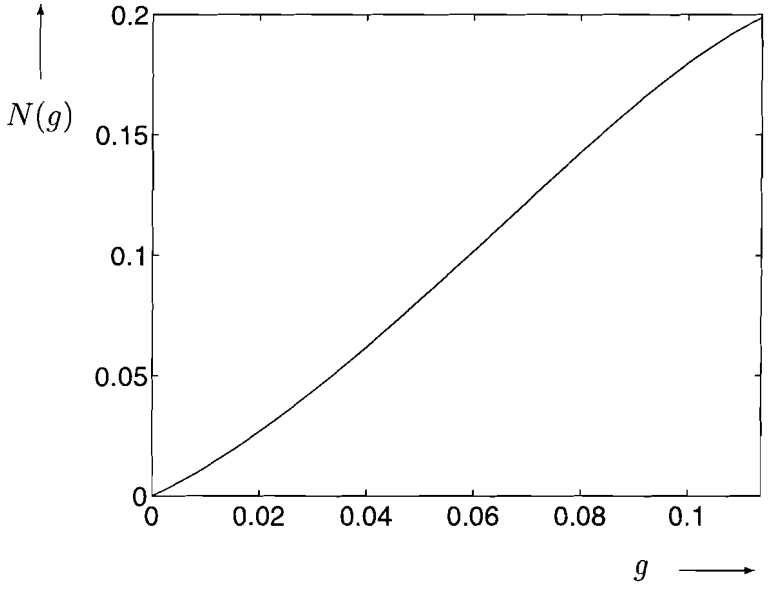

Figure 8: The function $N(g)$ for $D(\theta)$ given by (26) with Table 2 parameter values.

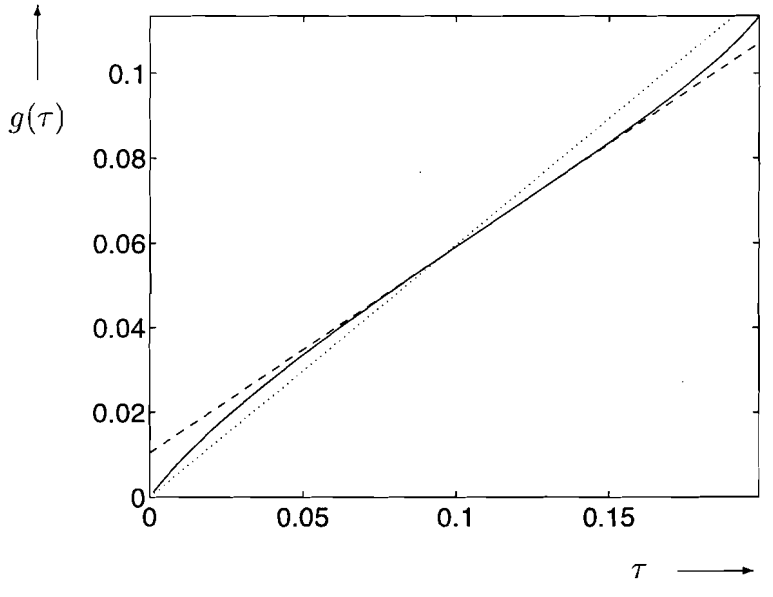

Figure 9: The function $g(\tau)$ which solves (38)–(39) for $D(\theta)$ given by (26) with Table 2 parameter values. The straight line approximations Approach 2 (42) with $g_0 = 0$ (dashed line) and Approach 3 (43) with $g_l = 0$ and $g_r = \frac{1}{2b_1 U}$ (dotted line) are shown.

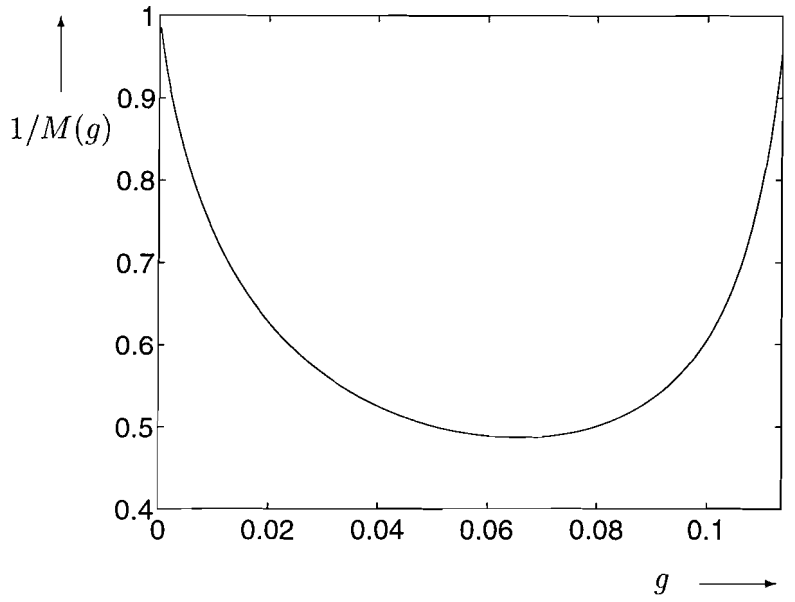

Figure 10: The function $1/M(g)$ for $D(\theta)$ given by (26) with Table 2 parameter values.

Approach 1

It is instructive to rewrite (37) as

$$\frac{dg}{d\tau} = \frac{1}{M(g)}.$$

Now we consider the graph of $1/M(g)$ in Figure 10. Denote $g = g_m$ to be the turning point of $1/M(g)$. Hence g_m satisfies

$$M'(g_m) = K_1 \ln\left(\frac{g_m}{K_1 g_m + 1}\right) + \frac{K_1}{K_1 g_m + 1} + K_2 = 0\,. \tag{40}$$

Then a linear approximation for $g(\tau)$ near g_m is

$$g(\tau) \approx g_0 + \frac{\tau}{M(g_m)}\,.$$

Since the function $1/M(g)$ is fairly flat near g_m, the slope is quite accurate over a significant interval for g.

Approach 2

This time we expand the integrated function $N(g)$ about $g = g_m$. Since g_m is defined in (40), it is the inflection point of $N(g)$. From the definitions of $N(g)$, $M(g)$ and $N''(g_m) = M'(g_m) = 0$, the Taylor series expansion gives

$$N(g) = N(g_m) + M(g_m)(g - g_m) + R(g)\,, \tag{41}$$

where $R(g)$ is a remainder term which can be estimated from

$$|R(g)| \leq \frac{1}{6}\max\left|\frac{d^2M}{dg^2}\right|(g-g_m)^3 .$$

By combining (38) and (41), we obtain the approximation

$$g(\tau) \approx \frac{\tau}{M(g_m)} + g_m + \frac{N(g_0)-N(g_m)}{M(g_m)} , \tag{42}$$

where we have ignored the non-linear remainder term $R(g)/M(g_m)$. In Figure 9, this straight line approximation is compared to the correct $g(\tau)$. Estimates of the size of the remainder show that it is small compared to the linear terms.

Approach 2 is a more sophisticated version of Approach 1. However both these approaches still involve solving a non-linear equation (40) each time. Next we describe a third and final approach – it is an averaging technique which only involves function evaluation.

Approach 3

This time an average value of the slope $dg/d\tau$ is calculated. Since it is too difficult to integrate $1/M(g)$ over a range of values of g, we invert the expression as

$$\frac{d\tau}{dg} = M(g).$$

Then define an average slope over an interval $g_l < g < g_r$, where we are free to choose appropriate values of g_l and g_r. For example, g_r can be equal to some fraction of $\frac{1}{b_1U}$, or g_m, although then a root of a non-linear equation must again be found. The advantage of choosing g_r in terms of $\frac{1}{b_1U}$ is that only function evaluations are needed. The natural value for g_l is g_0. The average is defined to be

$$Av\left[\frac{d\tau}{dg}\right] \doteq \frac{1}{g_r-g_l}\int_{g_l}^{g_r} M(g)\,dg = \frac{N(g_r)-N(g_l)}{g_r-g_l} .$$

Then an estimate for $g(\tau)$ can be made using this average slope as

$$g(\tau) \approx g_0 + \frac{g_r-g_l}{N(g_r)-N(g_l)}\,\tau . \tag{43}$$

Various choices of g_l and g_r can be explored. In Figure 9 the straight line approximation (43) with $g_l = 0$ and $g_r = \frac{1}{2b_1U}$ is displayed.

These three approaches all give similar estimates for the slope of a straight line fit to $g(\tau)$. The position of the front is just a multiple of $g(\tau)$ given by (36), and from the analysis here we have that its speed is

$$\frac{d\delta}{d\tau} \approx \frac{b_1U}{M(g_m)} \quad \text{or} \quad \frac{d\delta}{d\tau} \approx b_1U\frac{g_r-g_l}{N(g_r)-N(g_l)} .$$

Both Approach 1 and Approach 2 yield the first of these estimates, while Approach 3 yields the second. It is clear that the position of the front looks linear as it moves through a major fraction of the brick length.

More generally using (21) and (35), contours of constant values of ψ are given by

$$\xi = b_1(V(\psi) + U)g(\tau) \; .$$

Again there are constraints on the range of $g(\tau)$ applicable, because $0 < \xi < 1$. Since $g(\tau)$ is well approximated by a linear function of τ, each of these contours moves linearly into the brick for a fraction of the domain length.

6.3 Correction to solution $\theta > \theta_m$

As noted previously, this analysis gives an approximation (28) to the solution that has a constant flux $G(\tau)$. In particular this implies that at the physically insulated end $\xi = 1$, this approximation has a nonzero value of $\frac{\partial \psi}{\partial \xi}(1,\tau)$. From (28), we obtain

$$\frac{\partial \psi}{\partial \xi}(1,\tau) = \frac{G(\tau)}{1 - b_1 U + b_1 G(\tau)} = \frac{1}{b_1}\left[\frac{1}{1 + (1 - b_1 U)g(\tau)}\right] \; ,$$

while the required solution satisfies $\frac{\partial \bar{\theta}}{\partial \xi}(1,\tau) = 0$. For $0 < g < \frac{1}{b_1 U}$, we obtain

$$\min(\frac{1}{b_1}, U) < \frac{\partial \psi}{\partial \xi}(1,\tau) < \max(\frac{1}{b_1}, U) \; .$$

Since the value of b_1 is large, while U is small ($U \approx 0.11$ and $b_1 U > 1$ for Table 2 parameter values), the bounds of the slope of the approximate solution are small, so that the error in the slope is small. However, we still need to investigate the errors in the corresponding moisture profiles.

In Figure 11 a typical pseudo-steady state moisture profile $\psi(\xi,\tau)$ is plotted together with a numerically generated solution $\bar{\theta}(\xi,\tau)$ for the same value of τ. In comparing these two, we see that the general shape of the curves is identical, except for ξ near unity, where the difference is anticipated due to the flux discrepancy. We note that the difference in the two solutions is linear for $\theta > \theta_m$, and is negligible for $\theta < \theta_m$, as shown in Figure 11. We will show that this difference has little affect on the speed of the drying front.

These observations suggest that we write down a corrected approximate solution denoted by ψ_c, defined as

$$\psi_c(\xi,\tau) = \psi(\xi,\tau) - \begin{cases} \epsilon(\tau)\,[G(\tau)\xi - U] & , \quad \xi \geq \delta(\tau) \; , \\ 0 & , \quad \xi \leq \delta(\tau) \; , \end{cases}$$

showing the subtraction of a linear term in ξ for $\psi \geq \theta_m$. The coefficient $\epsilon(\tau)$ will be chosen so that the corrected solution satisfies a no-flux condition at $\xi = 1$. However, the

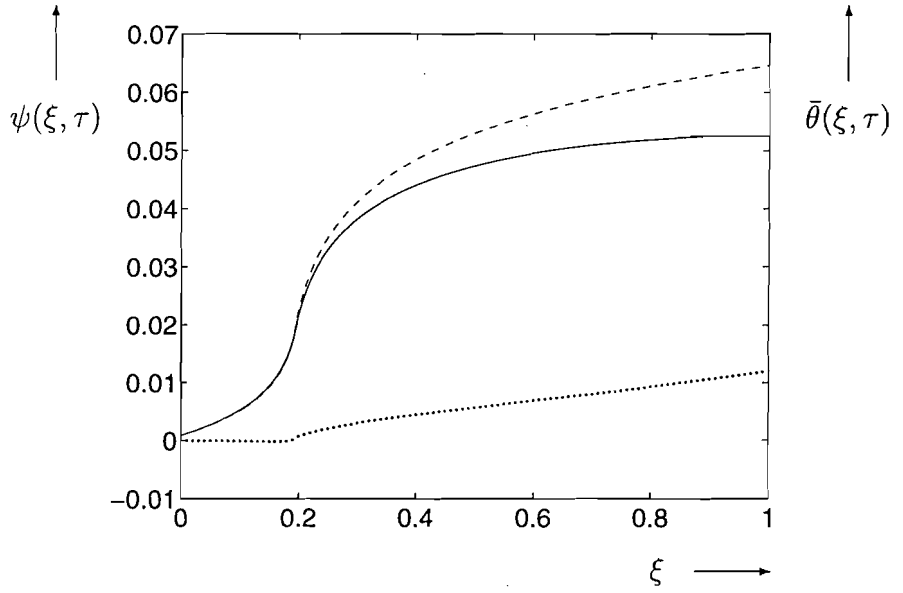

Figure 11: The moisture profile $\psi(\xi,\tau)$ (dashed line) and $\bar{\theta}(\xi,\tau)$ (solid line) for $D(\theta)$ given by (26) with Table 2 parameter values, both for $\tau = 0.03$. The difference $\psi(\xi,\tau) - \bar{\theta}(\xi,\tau)$ is also illustrated (dotted line).

position δ will be slightly different for uncorrected and corrected approximate solutions, as we shall see. To determine δ from (36), we again need to determine the time behaviour of $G(\tau)$ using the corrected approximation.

We have introduced this corrected approximation in order to satisfy the no-flux boundary condition at $\xi = 1$, hence it follows that we choose $\epsilon(\tau)$ as

$$\epsilon(\tau) = \frac{1}{1 - b_1 U + b_1 G(\tau)} = \frac{1}{K_1 + 1/g(\tau)}.$$

Using this corrected approximation ψ_c instead of ψ in (32), we again obtain a differential equation, which we write in the form

$$M_c(g)\frac{dg}{d\tau} = 1\ , \tag{44}$$

where the function $M_c(g)$ is a modification to the previous function $M(g)$ as

$$M_c(g) = M(g) - \frac{g}{2K_1}\left(\frac{1}{(1+K_1 g)^2} - (1-K_1)^2\right)\ .$$

The function $M_c(g)$ has the same qualitative behaviour as $M(g)$, so that it is a positive function with

$$M_c(0) = M(0) \quad , \quad M_c(\frac{1}{b_1 U}) = M(\frac{1}{b_1 U})\ .$$

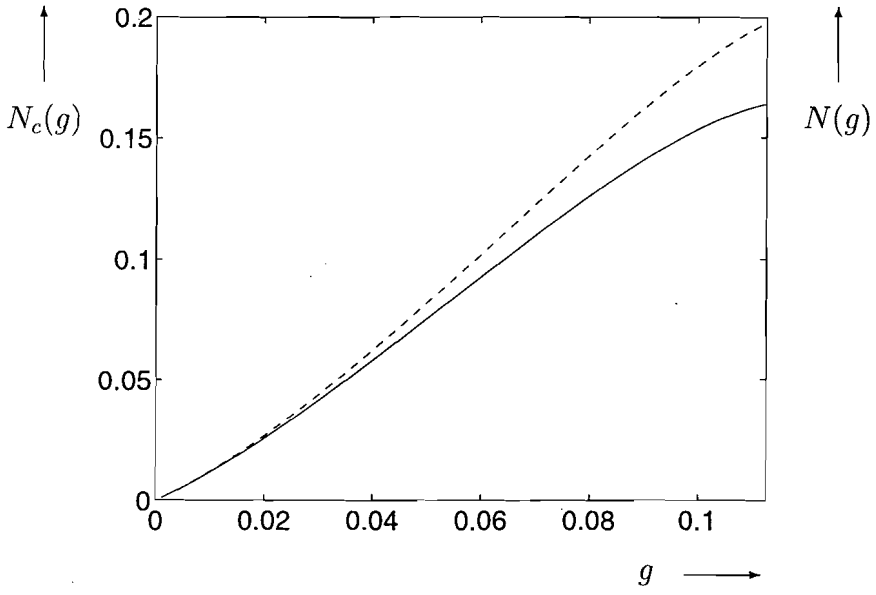

Figure 12: The functions $N_c(g)$ (solid line) and $N(g)$ (dashed line) for $D(\theta)$ given by (26) with Table 2 parameter values.

This behaviour again implies that $g(\tau)$ will be a increasing function of time. The equation (44) can be integrated to give

$$N_c(g) = \tau + N_c(g_0) \,, \tag{45}$$

where

$$\begin{aligned} N_c(g) &= \int_0^g M_c(f)\, df \\ &= N(g) - \frac{1}{2K_1^3}\left[\ln(1+K_1 g) - \frac{K_1 g}{1+K_1 g} - \frac{K_1^2(1-K_1)^2 g^2}{2}\right] , \end{aligned} \tag{46}$$

where $N_c(g_0)$ is the integration constant. N_c is a positive function of the two constants $b_1 U$ and d, through the constants K_1 and K_2 (see Figure 12).

Determining $g(\tau)$ and $\delta(\tau)$ proceeds in the same way as previously, where now the functions M and N are replaced by their corrected versions M_c and N_c. Again accurate estimates of these functions can be made using the similar methods as outlined in Approach 1 to 3. These are shown in Figure 13.

The true front position together with our approximations described in Section 6.1 and the corrected one outlined here are illustrated in Figure 14. It is clear that both approximations are excellent until the front is half-way through the brick. However the front position from the corrected approximation is closer to the true front position for a longer time (until the front is around 80% through the material). Consequently, the front speed

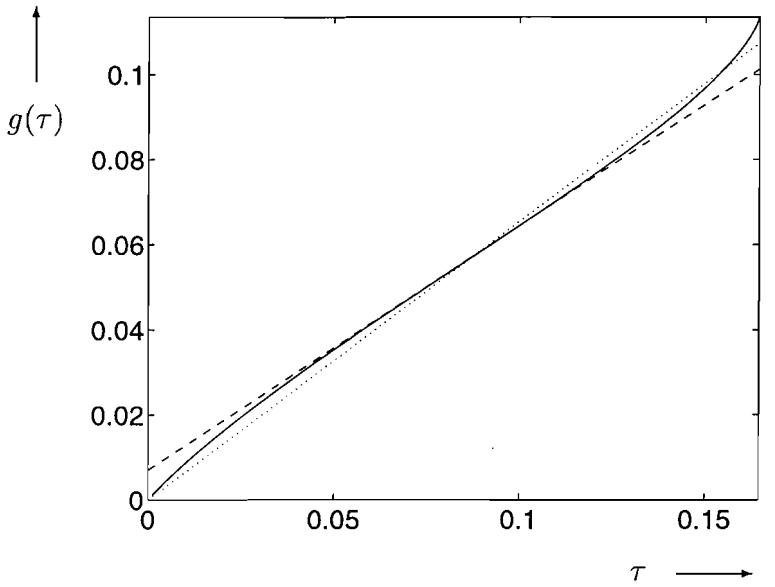

Figure 13: The function $g(\tau)$ which solves (45)–(46) for $D(\theta)$ given by (26) with Table 2 parameter values. The straight line approximations Approach 2 with $g_0 = 0$ (dashed line) and Approach 3 with $g_l = 0$ and $g_r = \frac{1}{2b_1 U}$ (dotted line) are shown.

obtained from the corrected approximation is a more accurate estimate of the true front speed. Hence, to obtain more accurate moisture profiles, it is necessary to use the corrected approximation provided by $\psi_c(\xi, \tau)$.

In Figure 15 the approximations ψ and ψ_c are compared with the numerically calculated $\bar{\theta}$. It can be concluded that ψ_c and $\bar{\theta}$ match very well. Similar comparisons with other fitting parameters indicate that ψ_c is a good approximation of $\bar{\theta}$ for moisture diffusivities with a clear and deep minimum.

Since the corrected function ψ_c is an excellent approximation to the numerical solution which represents $\bar{\theta}$, the validity of the assumption (24) can now be checked. Essentially, since $\bar{\theta} - \psi_c \approx 0$, we have

$$\left| \int_0^1 \frac{\partial(\psi - \bar{\theta})}{\partial \tau} \, d\xi \right| \approx \left| \int_0^1 \frac{\partial(\psi - \psi_c)}{\partial \tau} \, d\xi \right| \ll G(\tau) \, . \tag{47}$$

It follows from the definitions of ψ_c and M_c that

$$\int_0^1 \frac{\partial(\psi_c - \psi)}{\partial \tau} \, d\xi = \frac{g'(\tau)}{b_1 g(\tau)} \left(M(g(\tau)) - M_c(g(\tau)) \right) \, ,$$

and therefore (47) comes down to the inequality

$$\left| \frac{M(g) - M_c(g)}{M(g)} \right| \ll 1 \, .$$

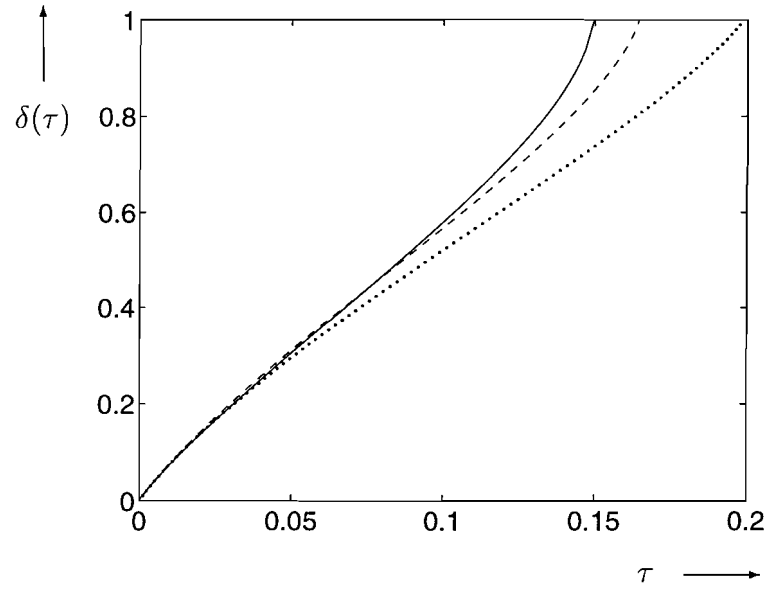

Figure 14: Position of the front as defined by $\bar{\theta}(\xi,\tau) = \theta_m$ (solid line) and the original (dotted line) as well as corrected (dashed line) $\delta(\tau)$ for $D(\theta)$ given by (26) with Table 2 parameter values.

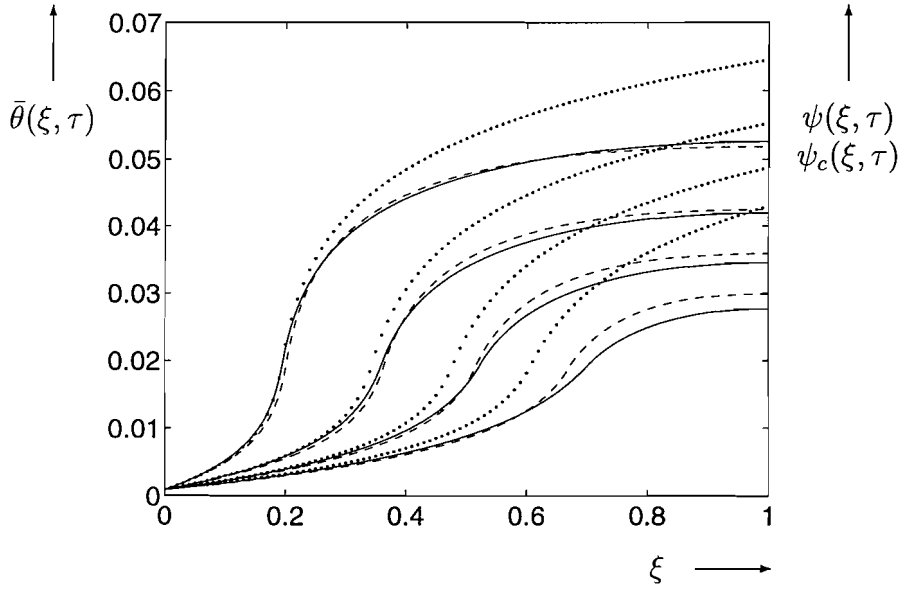

Figure 15: The moisture profiles $\bar{\theta}(\xi,\tau)$ (solid line), $\psi(\xi,\tau)$ (dotted line) and $\psi_c(\xi,\tau)$ (dashed line) for $D(\theta)$ given by (26) with Table 2 parameter values. Here τ has values 0.03, 0.06, 0.09 and 0.12.

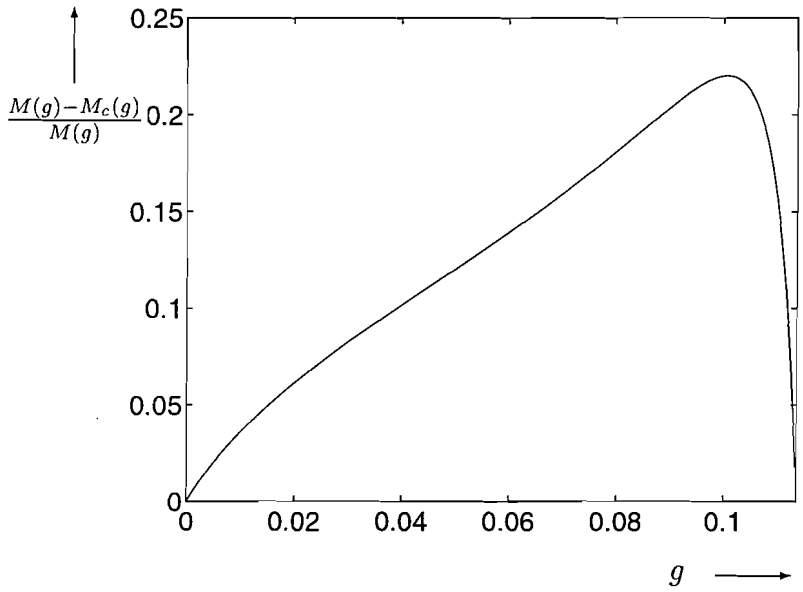

Figure 16: The function $(M(g) - M_c(g))/M(g)$ for $D(\theta)$ given by (26) with Table 2 parameter values.

The left-hand side of this inequality is plotted in Figure 16. It can be observed that a maximum of 0.22 is obtained.

It is also interesting to investigate the value of ψ_c at the internal no-flux boundary, namely

$$\psi_c(1,\tau) = \theta_m + \frac{1}{b_1}\left(\ln\left[1 - b_1 U + \frac{1}{g(\tau)}\right] - \frac{1 - b_1 U g(\tau)}{1 + (1 - b_1 U) g(\tau)}\right) .$$

As illustrated in Figure 17, the shape of this internal moisture content has essentially the same shape as the numerically calculated $\bar{\theta}(1,\tau)$.

7 Application to a diffusivity function with no interior minimum

As discussed earlier, often drying problems were assumed to be governed by a simple growing exponential diffusivity. Consequently we consider here

$$D(\theta) = A_1 e^{b_1 \theta} . \tag{48}$$

For this case the minimum value of D corresponds to the moisture content at the drying end, so that $\theta_m = \theta_\infty$. This identification in (26) reproduces this single exponential. Typically the diffusivity changes by orders of magnitude, so b_1 is assumed to be large. For this case, the analysis of the previous example remains the same, acknowledging that there is

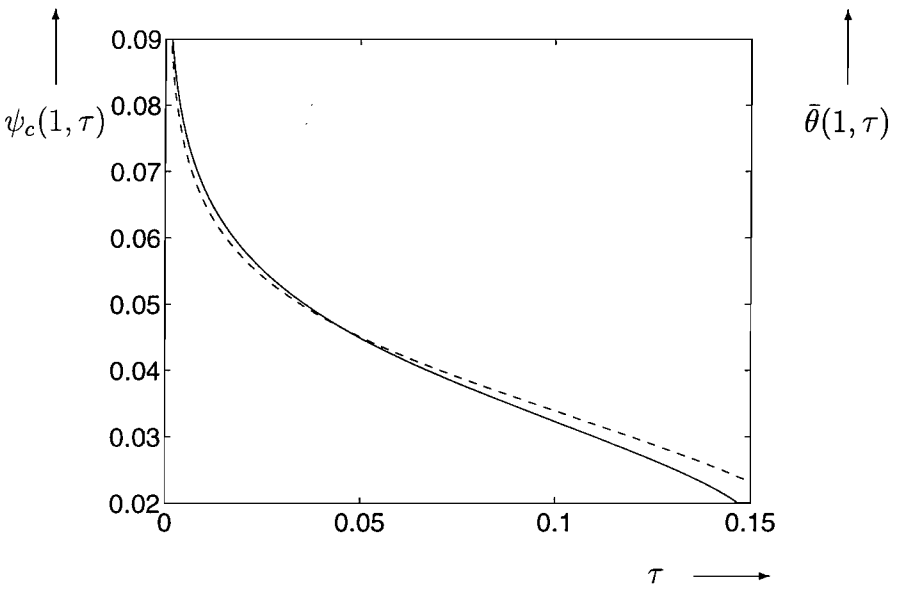

Figure 17: The moisture profiles $\psi_c(1,\tau)$ (dashed line) and $\bar{\theta}(1,\tau)$ (solid line) for $D(\theta)$ given by (26) with Table 2 parameter values.

no region where $\theta < \theta_m = \theta_\infty$, while now $U = 0$ and $\delta = 0$. Again we point out that at this stage the evolution of $G(\tau)$ with τ has not been determined. On physical grounds we expect it to be a positive decreasing function.

To determine the differential equation for $G(\tau)$ or equivalently $g(\tau)$, we consider (44) and (45) with $U = 0$, $K_1 = 1$, and $K_2 = 0$. Everything goes through smoothly to give

$$P(g)\frac{dg}{d\tau} = 1 \,,$$

where

$$P(g) = 1 - g\ln\left(1+\frac{1}{g}\right) - \frac{g}{2(1+g)^2} \,,$$

which on integration yields

$$Q(g) = \tau + Q(g_0) \,,$$

where

$$Q(g) = \int_0^g P(f)\, df = \frac{1}{2}\left[g - g^2\ln\left(1+\frac{1}{g}\right) + \frac{g}{1+g}\right] \,.$$

It is easy to verify that the function $Q(g)$ is a monotonically increasing function for all values of g. Numerical solution of these equations provides $g(\tau)$ as shown in Figure 18.

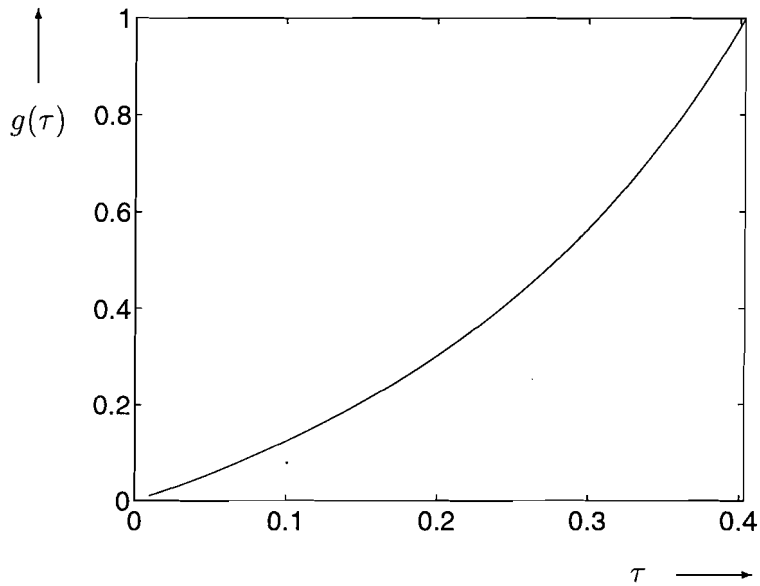

Figure 18: The function $g(\tau)$ for $D(\theta)$ given by (48) with Table 2 parameter values and $g_0 = 0$.

Asymptotics on the function Q for small values of g show that $g(\tau) \sim \tau$. However, unlike the previous example, Figure 18 shows that this linearity is restricted to a very local region near $\tau = 0$ only. Asymptotics on the function Q for larger values of g give $g(\tau) \sim e^{2\tau}$.

The corrected approximate moisture profile ψ_c can again be compared with the numerically generated $\bar{\theta}$ (see Figure 19). Notice now that the slope of the moisture profiles decreases as ξ increases and that there is no inflection point. Unlike the previous case, when the diffusivity had an interior minimum, clearly nothing resembling a front exists now. It can be seen that ψ_c has the same qualitative behaviour as $\bar{\theta}$. However, the match is not so good as in the case of a diffusivity function with an interior minimum. We do not pursue trying to improve the approximation, since we are not interested in the details of this case. The object here was to demonsrate that no drying front exists for this type of diffusivity function, and that the moisture profiles have a completely different shape.

Contours of constant values of ψ_c are given by

$$\xi = b_1 V(\psi_c) g(\tau) ,$$

and since $g(\tau)$ behaves exponentially (except for very small values of τ where it behaves linearly), this behaviour is quite different from the previous example with a minimum in the diffusivity function.

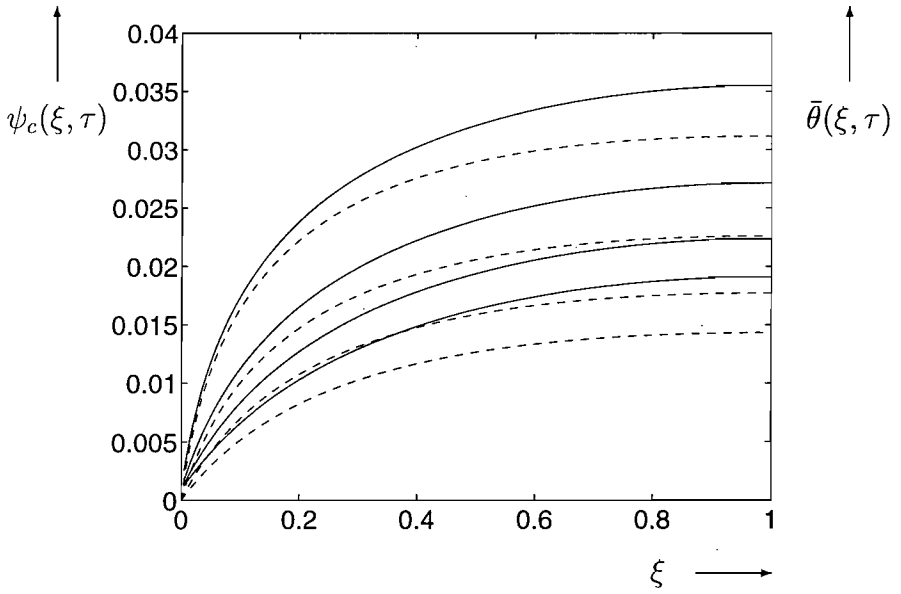

Figure 19: The moisture profiles $\psi_c(\xi,\tau)$ (dashed line) and $\bar{\theta}(\xi,\tau)$ (solid line) for $D(\theta)$ given by (48) with Table 2 parameter values. Here τ has values 0.03, 0.06, 0.09 and 0.12.

8 Discussion and conclusions

We have presented a simple model of the drying of a porous material. By comparing the relative time scales in the process, asymptotic analysis has shown that there are two distinct phases in the drying behaviour of bricks. In the first short stage the brick offers no resistance to the water motion. The behaviour is governed by the surface resistance and the moisture content is relatively uniform.

After this initial stage the boundary condition acts like a fixed moisture content condition. The drying behaviour is governed by non-linear diffusion. These equations can be solved numerically for the case when the diffusivity function contains a deep interior minimum. The results show that there is a drying front moving with an almost constant speed into the material.

In order to seek a greater understanding of the features of the numerical solutions, and the speed of the drying fronts, some asymptotic techniques have been used to explore the nature of the moisture profiles and front position. We have obtained a explicit expression for the moisture profiles in terms of the flux function $G(\tau)$. A differential equation is used to describe the evolution of this function with time.

By examining the effects of a diffusivity function with and without an interior minimum, we have shown that the presence of an interior minimum determines the existence of a drying front travelling into the brick. The position of the drying front is given implicitely

in terms of a nonlinear equation. However we have shown that the speed of the drying front is well approximated by a constant given by $b_1 U/M_c(g_m)$ in dimensionless units. This translates to an approximate speed of

$$v = \frac{b_1 \int_{\theta_\infty}^{\theta_m} D(\theta)\, d\theta}{L M_c(g_m)} \,. \tag{49}$$

The integral term is the area under the exponentially decreasing part of the diffusivity function, from the equilibrium moisture content to the value corresponding to the minimum diffusivity. Hence there are two important parts which contribute to the front speed – one is the exponent of the growing exponential b_1 and the other is the area under the exponentially decreasing part of the diffusivity function, as described here. Hence, both the decreasing and increasing branches of the diffusivity function contribute to the front speed.

This result gives an estimate of the time for drying a fraction f of the total sample length L as approximately

$$\frac{M_c(g_m)}{b_1 \int_{\theta_\infty}^{\theta_m} D(\theta)\, d\theta} L^2 f \,.$$

Notice that this implies that the time taken is proportional to $L^2 f$. This is quite different from the usual square-root time behaviour for diffusive processes, where the time is proportional to $L^2 f^2$.

The fitting parameters in Table 2 lead to $v = 0.04$ mm s^{-1}. This is slower than the experimentally measured speed of 0.06 mm s^{-1} (see Figure 3). This discrepancy is because our fitted diffusivity function is not an accurate enough approximation to the data for small θ values (see Figure 6). If A_2 and b_2 are chosen to give a more rapid decrease in the diffusivity at low θ values (e.g. $A_2 = 1.0 \cdot 10^{-2}$ mm^2 s^{-1} and $b_2 = 250$) then the approximate speed in (49) matches the experimentally observed front speed. It should be noted that our estimate of the speed is an accurate approximation of the front speed obtained for the numerically calculated profiles $\bar{\theta}$.

Moreover, we see that the moisture content solutions are a function of the variable $G(\tau)\xi - U$ or written another way, of $\xi - b_1 U g(\tau)$. Hence not only is the drying front travelling with a constant speed, but the solution behaves like a similarity solution, that it is stretched linearly in time.

It can be concluded that our analysis of the moisture content has the same qualitative features as the experimentally observed behaviour. Moreover, numerically generated solutions with our choice of diffusivity with a deep minimum can be approximated well with our asymptotically calculated corrected approximation $\psi_c(\xi, \tau)$. Furthermore, an accurate expression for the front velocity can be obtained in terms of the parameters in the problem.

Acknowledgments: Kerry Landman acknowledges financial support from University of Melbourne, and Eindhoven University of Technology and wishes to thank the Eindhoven University of Technology for their hospitality. Leo Pel was supported by the Dutch Technology Foundation (STW).

Table 1. Typical data values for fired clay brick

symbol	value	unit
L	25	mm
θ_0	0.25	–
θ_m	0.01 – 0.02	–
θ_∞	$9.14 \cdot 10^{-4}$	–
β	$6.36 \cdot 10^{-4}$	mm s^{-1}
h_a	0.61	–
$h_m(\theta_0)$	1	–
$h'_m(\theta_0)$	0.61	–
$h'_m(\theta_\infty)$	$1.45 \cdot 10^3$	–
$D(\theta_0)$	5.41	mm^2 s^{-1}
$D(0.1)$	~ 0.1	mm^2 s^{-1}
$D(\theta_m)$	$\sim 3 \cdot 10^{-4}$	mm^2 s^{-1}
$D(\theta_\infty)$	~ 0.01	mm^2 s^{-1}

Table 2. Typical fitting parameters for diffusivity function

symbol	value	unit
A_1	$5.0 \cdot 10^{-5}$	mm^2 s^{-1}
A_2	$5.0 \cdot 10^{-3}$	mm^2 s^{-1}
b_1	80	–
b_2	150	–

References

[1] J. BEAR and Y. BACHMAT, *Introduction to Modelling of Transport Phenomena in Porous Media*, Kluwer, Dordrecht (1990).

[2] D. BERGER and D.C.T. PEI, *Drying of hygroscopic capillary porous solids*, International Journal of Heat and Mass Transfer **16** (1973), pp. 293–302.

[3] M. BOGDAN, B.J. BALCOM, T.W. BREMMER and R.L. ARMSTRONG, *Single point imaging of partially dried hydrated white portland cement*, Journal of Magnetic Resonance A **116** (1995), pp. 266–269.

[4] P. BROADBRIDGE, J.H. KNIGHT and C. ROGERS, *Constant rate rainfall infiltration in a bounded profile: solutions of a nonlinear model*, Soil Science Society of America Journal **52** (1988), pp. 1526–1533.

[5] P. BROADBRIDGE, *Infiltration in saturated swelling soils and slurries: exact solutions for constant supply rate*, Soil Science **149** (1990), pp. 13–22.

[6] H.S. CARSLAW and J.C. JAEGER, *Conduction of Heat in Solids*, Oxford University Press, London (1959).

[7] T.A. CARPENTER, E.S. DAVIES, C. HALL, L.D. HALL, W.D. HOFF and M.A. WILSON, *Capillary water migration in rock: process and material properties examined by NMR imaging*, Materials and Structures **26** (1993), pp. 286–292.

[8] J. CRANK, *The Mathematics of Diffusion*, Oxford University Press, Oxford (1975).

[9] C.M. ELLIOTT, M.A. HERRERO, J.R. KING and J.R. OCKENDON, *The mesa problem - diffusion of patterns for* $u_t = \nabla \cdot (u^m \nabla u)$ *as* $m \to \infty$. IMA Journal of Applied Mathematics **37** (1986), pp. 147–154.

[10] G. GUILLOT, A. TROKINER, L. DARRASSE and H. SAINT-JALMES, *Drying of a porous rock monitored by NMR imaging*, Journal of Physics D: Applied Physics **22** (1989), pp. 1646–1649.

[11] K. LANDMAN and C.P. PLEASE, *Modelling moisture uptake in a cereal grain*, to appear in IMA Journal of Mathematics Applied in Business and Industry.

[12] M. MCGUINNESS, N. FOWKES, C.P. PLEASE, P. MCGOWAN, L. RYDER and D. FORTE, *Modelling the wetting and cooking of a single cereal grain*, to appear in IMA Journal of Mathematics Applied in Business and Industry.

[13] L. PEL, *Moisture Transport in Porous Building Materials*, PhD-Thesis, Eindhoven University of Technology (1995).

[14] L. PEL, H. BROCKEN and K. KOPINGA, *Determination of moisture diffusivity in porous media using moisture concentration profiles*, International Journal of Heat and Mass Transfer **39** (1996), pp. 1273–1280.

[15] J.R. PHILIP, *Numerical solution of equations of the diffusion type with diffusivity concentration-dependent II*, Australian Journal of Physics **10** (1957), pp. 29–42.

[16] J.R. PHILIP, *The theory of infiltration: 1. the infiltration equation and its solution*, Soil Science **83** (1957), pp. 345–357.

[17] J.R. PHILIP, *General method of exact solution of the concentration-dependent diffusion equation*, Australian Journal of Physics **13** (1960), pp. 1–12.

[18] J.R. PHILIP, *Theory of Infiltration*, Advances in Hydroscience **5** (1969), pp. 215–305.

[19] J.R. PHILIP, *On solving the unsaturated flow equation: 1. the flux-concentration relation*, Soil Science **116** (1973), pp. 328–335.

[20] J.R. PHILIP and D.A. DE VRIES, *Moisture movement in porous materials under temperature gradients*, Transactions of the American Geophysical Union **38** (1957), pp. 222–232.

[21] G.W. SCHRADER and J.B. LITCHFIELD, *Moisture profiles in a model food gel during drying: measurement using magnetic resonance imaging and evaluation of the Fickian model*, Drying Technology **10** (1992), pp. 295–332.

[22] M.A. STANISCH, G.S. SCHAJER and F. KAYIHAN, *A mathematical model for drying of hygroscopic porous media*, AIChE Journal **32** (1986), pp. 1301–1311.

[23] A.G.F. STAPLEY, *Diffusion and Reaction in Wheat Grains*, PhD-Thesis, University of Cambridge (1995).

[24] A.G.F. STAPLEY, L.F. GLADDEN and P.J. FRYER, *A study of diffusion and reaction in whole wheat grains during boiling*, AIChE Journal **44** (1986), pp. 1777–1789.

[25] K. VAFAI and M. SOZEN, *A comparative analysis of multiphase transport models in porous media*, Annual Review in Heat Transfer **3** (1990), pp. 145–165.

[26] K. WAANANEN, J.B. LITCHFIELD and M.R. OKOS, *Classification of drying models for porous solids*, Drying Technology **11** (1993), pp. 1–40.

[27] S. WITHAKER, *Simultaneous heat, mass and momentum transfer in porous media. A theory of drying porous media*, Advances in Heat Transfer **13** (1977), pp. 119–200.

[28] T.P. WITELSKI, *Stopping and merging problems for the porous media equation*, IMA Journal of Applied Mathematics **54** (1995), pp. 227–243.

[29] T.P. WITELSKI, *The structure of internal layers for unstable nonlinear diffusion equations*, Studies in Applied Mathematics **97** (1996), pp. 277–300.